Modular Isolated Soft-Switching Medium Voltage String Inverter for Large-Scale PV Farm

Zheng An, Xiangyu Han, Liran Zheng, Karthik Kandasamy, Rajendra Prasad Kandula, Deepak Divan
School of Electrical and Computer Engineering
Georgia Institute of Technology
Atlanta, the United States
zheng.an@gatech.edu

***Abstract*— This paper presents a single-stage modular isolated soft-switching medium voltage string inverter (MVSI) with tri-port configuration to interconnect PV and storage to medium voltage (MV) grid. The modular MVSI provides advanced functionalities such as energy storage elements integration without additional converters, connection to MV grid resulting in lower distribution losses in the PV farm, high-frequency galvanic isolation, independent control of PV, storage and grid power, high modularity and scalability. The topology of the MVSI, operation principle and model-predictive priority-switching (MPPS) control to achieve fast dynamic balancing across stacked modules are discussed. The independent power control is validated in PLECS simulation and the operation of stacked MVSI with MPPS control is verified through Hardware-in-the-loop (HIL) simulation. The hardware prototype of 25 kVA MVSI building block is developed. 18 kW experimental results of single building block verifying tri-ports operation and 20 kW experimental results of two modules stacked operation are presented. A clean sinusoidal waveform with negligibly low THD in both tests is obtained. A low dv/dt of < 1kV/us and soft-switching are achieved.**

Keywords—Soft-switching, medium voltage string inverter, tri-port, stacked operation.

I. INTRODUCTION

In the last decade, the price for utility-scale photovoltaic (PV) energy has been dropping exponentially, primarily driven by dropping prices of PV panels [1]. To further bring down the system price and satisfy the SunShot 2030 goal, another driver of cost decrease, i.e. the cost of 'balance of systems' (BOS), has gained attention [1][2]. One major component of BOS cost is the electrical components (EBOS), including current collection, power conversion, transformer isolation, and breakers. One way to reduce the EBOS is to change PV farm distribution of LVDC (1000 V DC) to MVAC (> 4 kV), which can reduce the copper loss in the farm distribution. Besides, MVAC distribution also presents an opportunity to replace the underground distribution with overhead distribution, which can be fulfilled at a reduced cost and time.

At present, central inverters are widely employed in utility-scale PV farms. The typical central inverters in such applications can output a megawatt-level power but a low line-to-line voltage per each, which causes a flowing current of up to thousands of amperes and consequently high copper loss. Moreover, a step-up line-frequency transformer is required to interface the central inverter to MVAC grid, which brings additional cost and loss [3]. Compared to central inverters, string inverters save the cost by eliminating combiner boxes and improved Operation and Maintenance (O&M) cost [4]. However, the string inverters have a limited output voltage up to 600 Vac, which induces high current collection and consequently similar copper loss as central inverters. And a line-frequency transformer is still required for isolation and voltage amplification when interfacing to the MV grid.

Alternatively, connecting the isolated string inverter modules in input-parallel output-series (IPOS) configuration is an attractive alternative to interconnect to MVAC grid while eliminating the bulky line-frequency transformer for cost and loss savings [5]-[7]. For the DC to MVAC application, two-stage inverters with bulky dc-link capacitors are dominant, where the dc-dc stage provides voltage amplification and galvanic isolation and dc-ac stage output sinusoidal waveforms, such as isolated cascaded half-bridge (CHB) converter [8]-[10]. There are also several single-stage inverters have been proposed [11]-[14]. However, there exist some drawbacks like bulky passive components, higher complexity to integrate storage, relatively higher loss, etc [8]-[15].

Recently, the utility-scale "PV-Plus-Storage" system has gained attention due to its provision of energy dispatchability and grid support services and cost benefits [16][17]. Consequently, a single-stage topology, which can integrate the PV and also storage without additional semiconductors, is preferred for its simplicity.

In this paper, a single-stage modular isolated soft-switching current-source MVSI is proposed, which provides storage units integration with no additional semiconductors, independent control of PV, storage and grid. And it can be easily connected in IPOS configuration to interconnect to MV grid with galvanic isolation. The topology, operation and control of the proposed MVSI are explained. And the independent power control and fast-dynamic control is validated by the PLECS and OPAL-RT HIL simulations, respectively. The system design and prototype development of 25 kVA MVSI building block are discussed. In the end, the 18 KW experimental results of single module and 20 kW of two modules stacked operation are presented to validate its functionalities.

II. MVSI IMPLEMENTATION

A. Topology and Operation

The proposed single-stage modular isolated soft-switching MVSI is derived from soft-switching solid-state transformer

The authors would like to thank DoE and Prolec for funding this research.

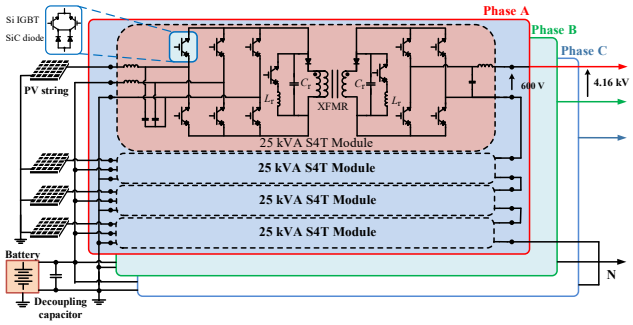

Fig. 1. 300 kVA S4T-based MVSI with battery storage.

(S4T) topology [18]. As shown in Fig. 1, the proposed MVSI consists of multiple S4T modules connected in the IPOS manner. Each S4T module is configured as a tri-port with PV and storage connected to the LV bridge. On the MV bridge, the S4T module is configured as a single-phase output for series stacking and multiple of the S4T modules are connected in series on the AC side to achieve MV. The three-phase system contains three of them in the same structure. It should be highlighted that a common storage/capacitor is connected across all the modules. The storage is not necessary for the converter operation and can be replaced by a small film capacitor, called the decoupling capacitor. A decoupling capacitor is required to eliminate double-line frequency pulsating power for dc to single-phase ac applications [19]. And the implementation of a common storage/capacitor allows the exchange of power across the modules, which guarantees a balanced output across the series-connected modules even when the inputs are unbalanced. The basic operation principle of S4T is analogous to the flyback converter [18], where the transformer magnetizing inductance L_m, i.e. the energy transfer element of S4T, gets charged from the power source and then dumps the energy to the output port successively. The resonant tanks connected to the transformer on both sides, which are composed of resonant capacitors C_r and resonant inductors L_r, enable the soft-switching transitions for all main devices. The resonant capacitor voltage V_{Cr} descends from the most positive voltages to the most negative ones sequentially and the resonant state is activated for half resonant cycle to flip the resonant capacitor voltage over to repeat for next switching cycle, like the example shown in Fig.2.

B. Control

The basic operation principle of the S4T based tri-ports converter has been introduced in [18][20]. The state sequences of active vectors V_{pv}, V_{cap} and V_{ac} and free-wheeling (FW) state V_{fw} are determined by the power flow direction and their voltage magnitude. In grid-forming mode, power flows from PV to the grid. PV is always a positive vector charging L_m and AC the negative one discharging L_m. The decoupling capacitor could be either a positive or negative vector depending on the double-line frequency pulsating power compensation requirement. As a result, there are three state sequences under the system specifications in this mode, i.e.

1) PV -> CAP -> FW -> AC;

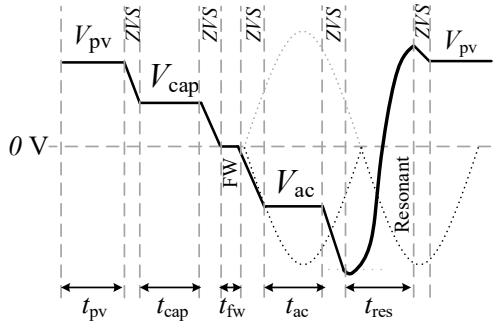

Fig. 2. Resonant capacitor voltage waveform with the state sequence PV -> CAP -> FW -> AC

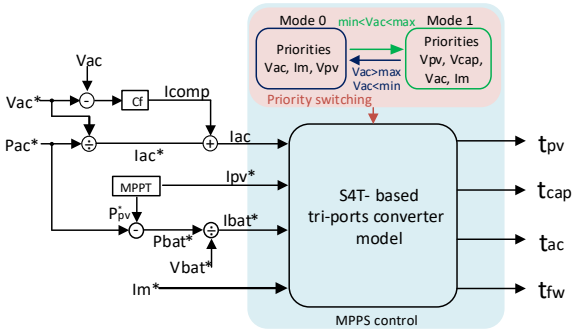

Fig. 3. The MPPS control diagram.

2) PV -> FW -> CAP -> AC;

3) PV -> FW -> AC -> CAP.

In grid-following mode, PV and grid supply power to energy storage port. Therefore, PV and AC vectors are positive vectors and the decoupling capacitor vector is the negative one. The state sequence is always PV -> AC -> FW -> CAP.

Due to the small magnetizing inductance and consequently low inertia property of S4T topology, the traditional control methods cannot manage the energy difference between I/O ports when a transient disturbance occurs. Therefore, a fast-dynamic control model-based control, namely Model-predictive priority switching (MPPS) control was proposed for stacked low-inertia converters [21]. Figure 3(a) shows the MPPS control diagram. The time duration of different states is calculated according to the magnetizing current reference I_m and tri-ports converter model and the state sequences are determined with priority switching strategy based on I/O voltage amplitudes, the power flow direction, and control objectives. The MPPS algorithm is implemented in DSP and after that the state machine is executed in FPGA to change switch states to achieve the control goals.

C. System Design

The MVSI building block is rated at 25 kVA per each and the detailed parameters are summarized in TABLE I. The calculated magnetizing inductance with (1) is subjected to the average current 120 A and 0.6 p.u. maximum ripple current benefiting the control range. The resonant capacitors of 50 nF and resonant inductors of 2 uH are optimized to give a low dv/dt of 1 kV/us, reduced resonant time duration and decreased

TABLE I. SPECIFICATIONS OF 25 KVA MODULE

Parameters	Values
PV voltage	1000 V
AC voltage	600 Vrms
Battery voltage	650 V
Decoupling capacitor	1.1 mF
Switching frequency	16 kHz
Magnetizing inductance	350 uH
Resonant capacitor	50 nF
Resonant inductor	2 uH

$$L_{\mathrm{m}} = V_{\mathrm{L,max}} \cdot d_{\mathrm{eff}} \cdot T_{\mathrm{sw}} / (I_{\mathrm{m,avg}} \cdot 0.6) \quad (1)$$

$$d_{eff} = 1 - (t_{ZVS} + t_{res})/T_{sw} \quad (2)$$

$$C_r = 0.5 \cdot I_m/(dv/dt) \quad (3)$$

$$C_{decouple} = P_{dc}/(\omega_{line} \cdot V_{dc} \cdot \Delta v) \quad (4)$$

device stress [18][22][23]. The decoupling capacitor, which is paralleled with the battery storage units, takes responsibility for the pulsating power and therefore guarantees a flat dc power on the PV port for lifetime benefits. With the pre-defined 100V voltage ripple, the decoupling capacitor can be calculated by (4).

Four 25 kVA modules are stacked to form a 100 kVA / 2.4 kVrms single-phase ac system and 12 of them can compose a 300 kVA three-phase system. The compensated double-line frequency pulsating power in the decoupling capacitor will cancel out each other in a balanced three-phase system and therefore a small film capacitor is sufficient, which can minimize the capacitance size and weight, benefits a dc power throughput to the energy storage port like a battery unit and also improves the system reliability.

III. SIMULATION AND HARDWARE-IN-THE-LOOP RESULTS

A. 25 kVA Building Block

With the schematic shown in Figure 1 and parameters listed in Table 1, the PLECS simulation of 25 kVA MVSI building block are implemented and the results of four different cases in grid-forming and grid-following modes are presented in Fig. 4 to validate the independent power control of three ports.

Case 1: grid-forming mode with 100% load. PV and battery power flow into the grid;

Case 2: grid-forming mode with 50% load. PV power flows into the battery and grid;

Case 3: grid-forming mode with 50% load. No PV power and battery power flows into the grid;

Case 4: grid-following mode. PV power and grid power flow into the battery storage;

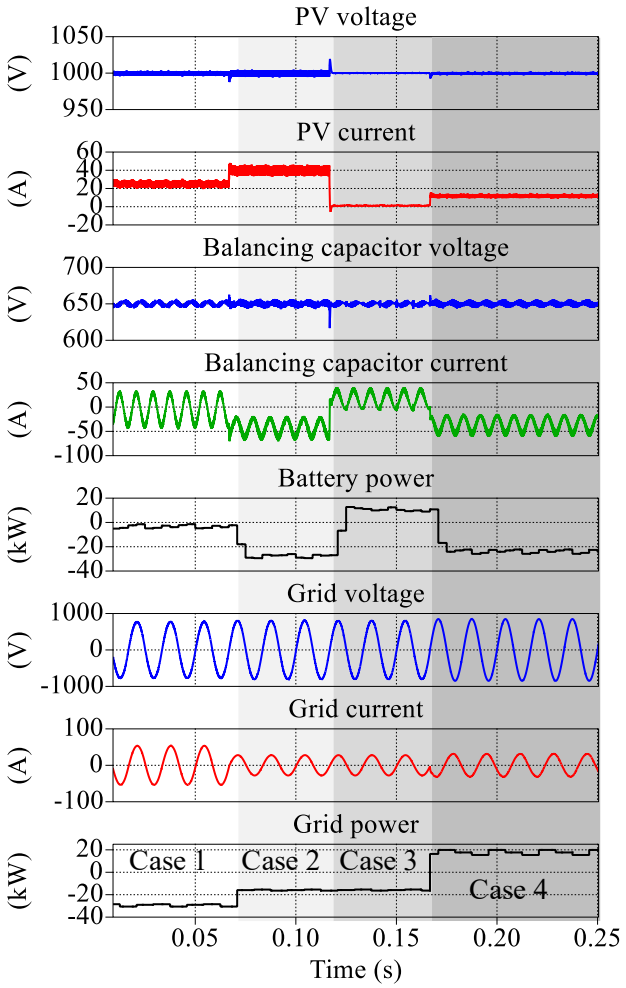

(a) The independent power control of PV, battery and grid ports.

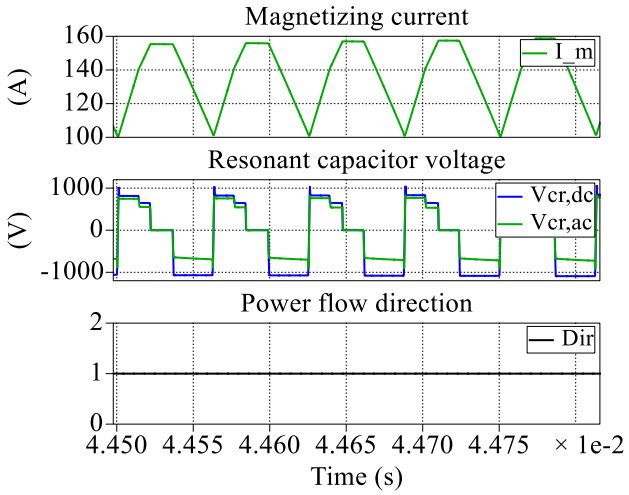

(b) Magnetizing current and resonant capacitor voltage in grid-forming mode.

Fig. 4. Simulation results of 25 kVA MVSI building block.

Fig. 4(a) validates the independent control of the PV, storage and grid power in three ports, where the decoupling capacitor power compensates the double-line frequency power pulsation and benefits a flat PV output. Fig. 4(b) shows the

state sequence in grid-forming mode and verifies the soft-switching capability.

B. *Two Modules Stacked Operation*

Figure 5 shows the HIL simulation of stacked two 25 kVA modules with the interleaved operation implemented on OPAL-RT platform. As shown in Fig. 5(a), two modules are controlled by two separate controllers with daisy change communication [24]. Fig. 5(b) – (d) presents the results under power ramp-up, steady-state and step load change conditions, respectively. The non-ideal parameters such as sensors delay, sensor bandwidth limitation, and parasitic elements are implemented in the HIL model to emulate the hardware prototype. The step load change is intentionally implemented to validate the fast- dynamic voltage balancing with the MPPS control in stacked operation.

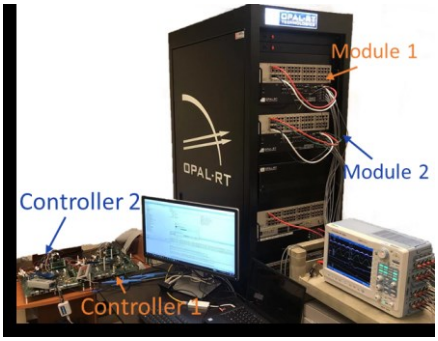

(a) HIL simulation setup

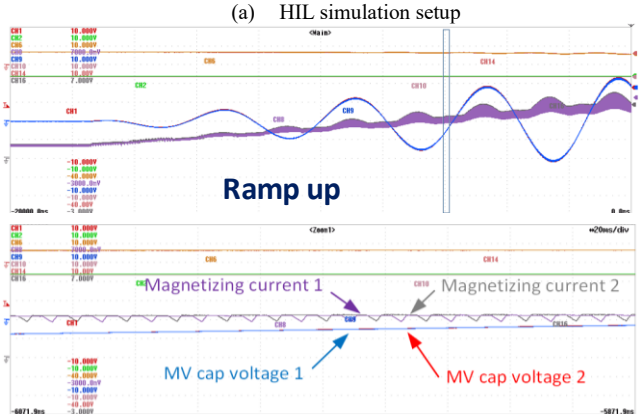

(b) Power ramp-up

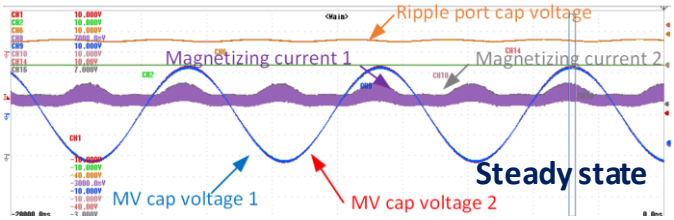

(c) Steady state

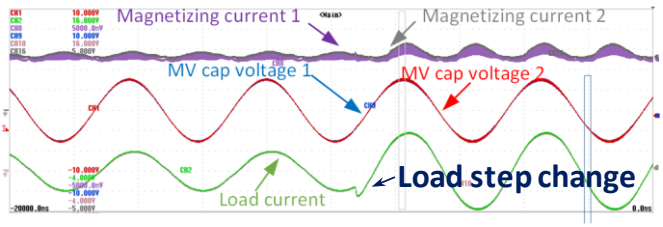

(d) Load step change

Fig. 5. HIL simulation of MVSI on OPAL-RT platrform. (MV cap voltage: 200 V/div; MV grid current: 15 A/div; Magnetizing current: 50 A/div; PV current: 30 A/div; Energy storage port current: 40 A/div.)

IV. PROTOTYPES BUILD

With the system specifications listed in Table I, the 25 kVA MVSI building block has been built and the selected Bill of Materials (BOM) is summarized in Table II.

A. *1.7 kV Reverse-blocking Device Block*

The switch used in the MVSI building block is a reverse-blocking device, which is composed of 1.7 kV silicon IGBTs and 1.7 kV silicon carbide diodes. Here the 1.7 kV silicon IGBT IXBK75N170 from IXYS and 1.7 kV SiC diode GB50MPS17-247 from GeneSiC is selected. And due to the limited current ratings, two of each device has to be connected in parallel to accommodate the magnetizing inductance current, as shown in Fig.6.

B. *Gate Drivers*

Customize-designed low-cost gate drivers with Under-Voltage Lock-Out (UVLO) protection are employed in MVSI building blocks and the prototypes are shown in Fig.7. The HV-side gate driver, which is used on the stacked ac side, receives the gate signal and sends the UVLO signal via fiber

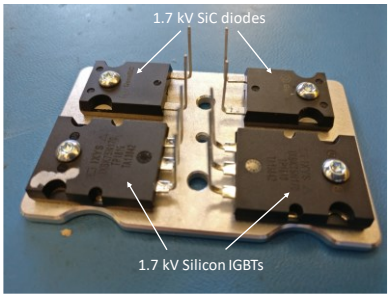

Fig. 6. 1.7 kV reverse-blocking device block

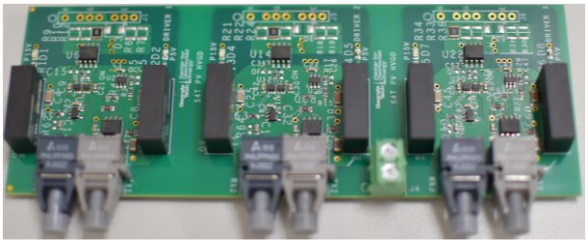

(a) HV-side gate driver

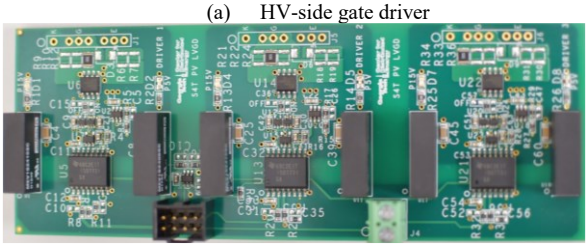

(b) LV-side gate driver

Fig. 7. Customized gate drivers

TABLE II. SELECTED BOM OF 25 KVA BUILDING BLOCK

Components	Part Number	Manufacturer
1.7 kV Si IGBT	IXBK75N170	IXYS
1.7 kV SiC diode	GB50MPS17-247	GeneSiC
Resonant capacitor	PHE450TB5100JB16R17	KEMET
Resonant inductor	Customized, N/A	Customized, N/A
Decoupling capacitor	947C731K801CDMS	Cornell Dubilier Electronics (CDE)
Transformer cores	SC2062M1	MK Magnetics
Permanent magnets	BY0X01/02/04	K&J Magnetics

optics, which works with an isolated gate driver power supply (GDPS) together to provide sufficient isolation capability. The LV-side gate driver used on dc side can withstand up to 5 kVrms voltage with the integrated capacitive coupled isolators.

C. DSP+FPGA Control Board

To implement the MPPS algorithm, a customized control board integrating the DSP and FPGA has been designed, where the DSP chip TMS320C6713B from TI and FPGA chip 10CL080YF484I7G from Altera are selected. The DSP takes responsibility for state sequence determination and time duration calculation while the FPGA executes the state machine, generates the gate signal and implements the fault and protection function.

D. 25 kVA High-frequency Transformer

The 350 uH, 25 kVA high-frequency transformer with two pairs of nanocrystalline cores SC2062M1 from MK Magnetics has been built. Since there always exists a dc flux on the transformer for the MVSI operation, a few permanent magnets are mounted around the airgap in opposite polarity to cancel out the flux and therefore increase the saturation current. The measured magnetizing inductance is 330 uH with 100 mils airgap on each side and the saturation current increases to 158 A compared to 75 A without the magnets.

E. 25 kVA MVSI Building Block Prototype

The assembled hardware prototype of the 25 kVA MVSI building block is shown in Fig.10. The prototype is equipped with air cooling and has a dimension of 36” L x 15” W x 7” H.

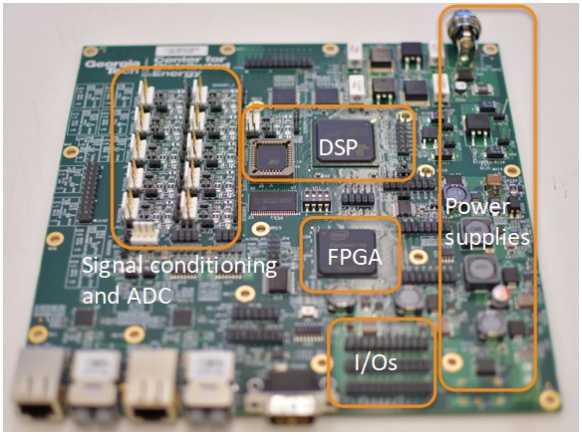

Fig. 8. Customized FPGA+DSP control board.

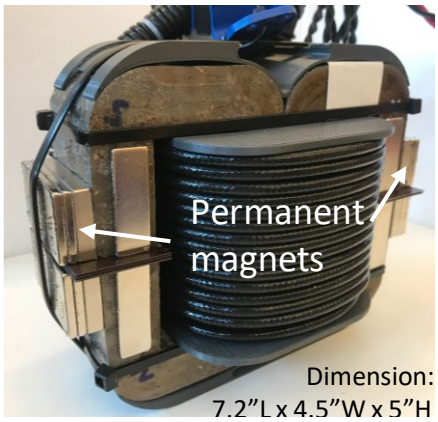

Fig. 9. 25 kVA hight frequency transformer with dc-bias.

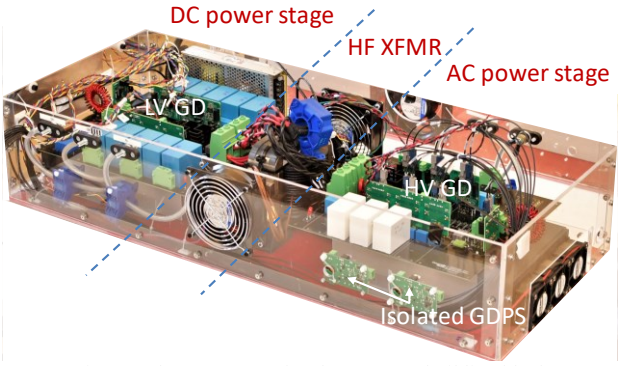

Fig. 10. The prototype of 25 kVA MVSI building block.

V. EXPERIMENTAL RESULTS

A. 25 kVA Building Block

The 25 kVA building block has been tested and 18 kW experimental results are presented in Fig.11. The magnetizing current, the green curve in Fig.11(a), is well controlled and the ac output current presents a clean sinusoidal waveform with negligible low total harmonic distortion (THD). Besides, thanks to the decoupling capacitor, PV voltage/current remains flat without suffering from double-line frequency pulsating power. Fig.11(b) shows the zoom-in resonant capacitor voltage with the state sequence of PV -> CAP -> FW -> AC at the ac peak current point, where a low dv/dt of less than 1 kV/us and the soft switching feature is observed. Fig.11(c) shows the zoom-in resonant capacitor voltage at the ac zero-crossing point with a different state sequence PV -> FW -> AC -> CAP. But both benefits of the soft-switching and low dv/dt < 1 kV/us still exist.

B. Two Modules Stacked Operation

The stacked operation of two 25 kVA modules with the MPPS control algorithm has been tested and the test setup is shown in Fig. 12, where module 1 is considered as the master module and module 2 as the slave module. The 20 kW experimental results with 10 kW per building block are presented in Fig.13. From Fig. 13(a), it can be observed that

the magnetizing current in both modules is well under control and the stacked ac output voltage and current present a clean sinusoidal waveform with low THD. Figure 13(b) and (c) shows the zoomed resonant capacitor voltages of two modules at ac peak current and zero-crossing points, respectively. Different state sequences are executed in these two operation

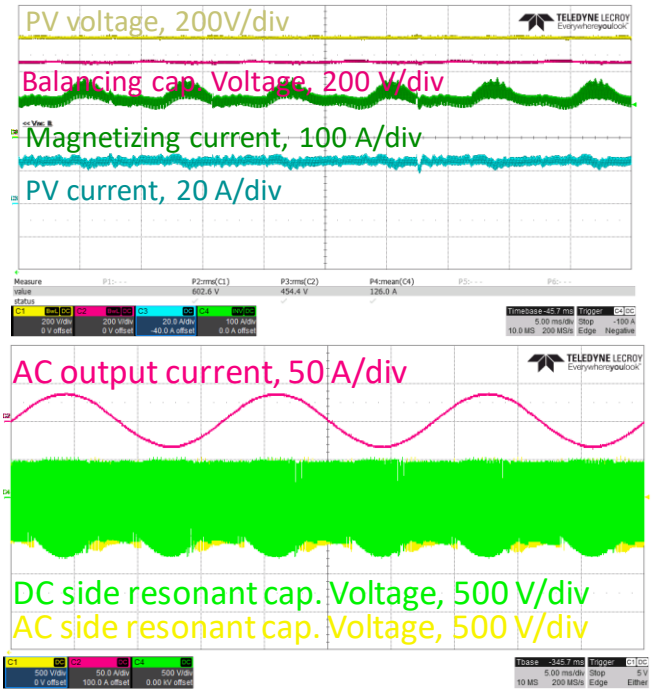

(a) Magnetizing current, I/O voltage/current and resonant capacitor voltages.

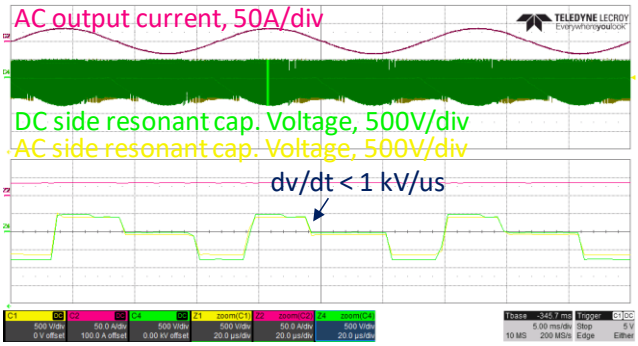

(b) Zoom-in view of resonant capacitor voltage at ac peak current.

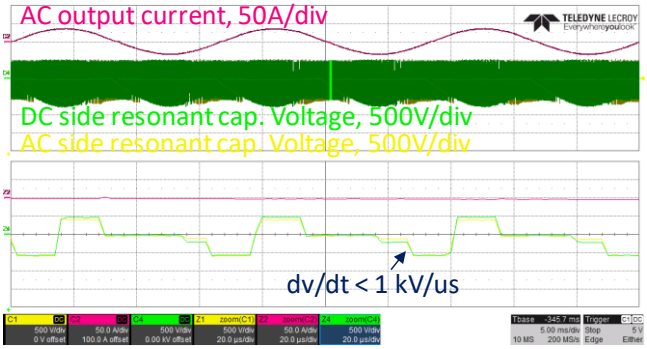

(a) Zoom-in view of resonant capacitor voltage at ac zero-crossing.

Fig.11. 18 kW experimental results of 25 kVA MVSI building block.

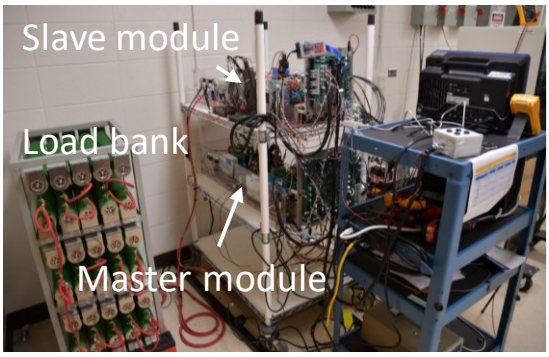

Fig.12. Test setup of two modules stacked operation.

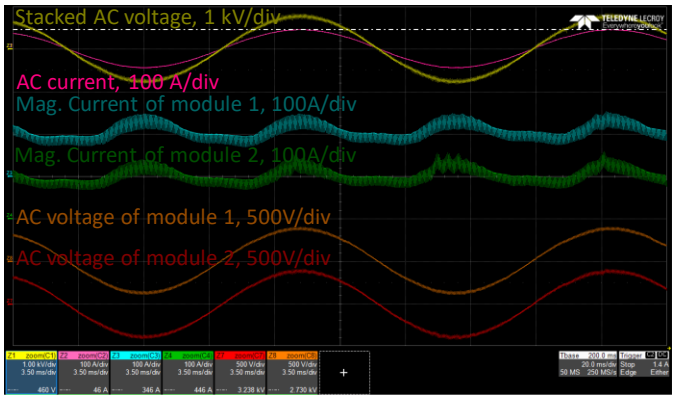

(a) Stacked ac output voltage and current, magnetizing current and ac output voltage of two modules.

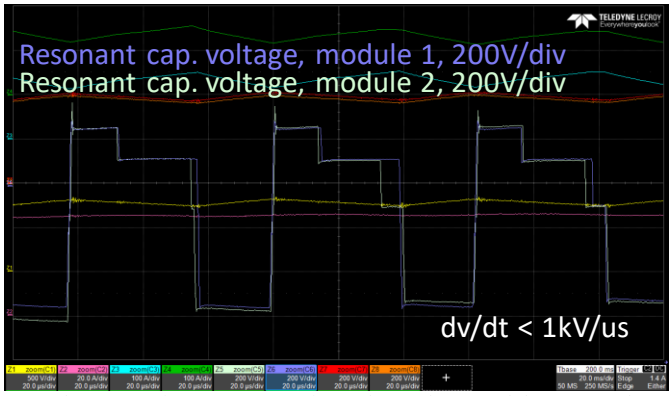

(b) Zoom-in resonant capacitor voltage of two modules at ac peak current point.

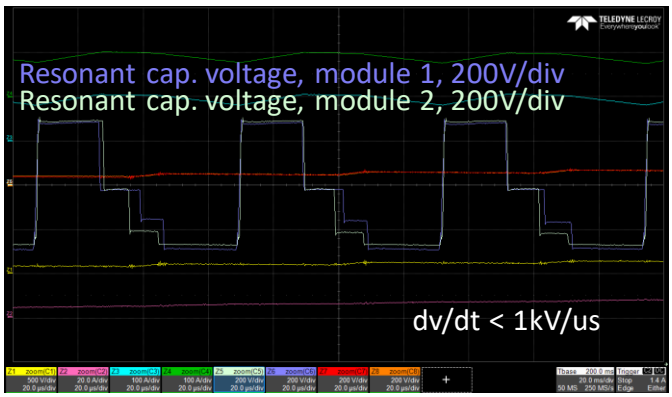

(a) Zoom-in resonant capacitor voltage of two modules at ac zero-crossing point.

Fig.13. 20 kW experimental results of two modules stacked operation.

points but both present a controlled low dv/dt of less than 1 kV/us and soft-switching feature.

VI. Conclusion

This paper presents a novel single-stage modular isolated soft-switching MV string inverter (MVSI) to reduce the losses and costs for large-scale PV farms applications. The tri-port configuration integrates the energy storage units to provide energy dispatchability and grid support services without adding any additional converter. The fast-dynamic MPPS control for the low-inertia MVSI and the system design of the MVSI is discussed. The independent power control of three ports is validated in PLECS simulation and the fast-response of MPPS control is verified with HIL simulation on the OPAL-RT platform. The hardware prototype of 25 kVA MVSI building block is developed with customized RB device block, gate drivers and FPGA+DSP control board. 18 kW experimental results of single MVSI building block as well as the 20 kW experimental results of two modules stacked operation are presented. In both experiments, sinusoidal ac outputs with negligibly low THD are observed. Besides, a low dv/dt of < 1kV/us and soft-switching is achieved at different operations points in both tests.

Acknowledgment

The authors would like to acknowledge Mickael Mauger, Xiwei Zheng, Brandon Royal, Joshua Boudreau, Zachary Laird and Jackson Daniel for their help with the prototype development.

References

[1] R. Fu, D. Feldman, and R. Margolis, "U . S . Solar Photovoltaic System Cost Benchmark : Q1 2018," Nrel, no. Novmnber, pp. 1–47, 2018

[2] U.S. DOE, "The SunShot 2030 Goals: 3¢ per Kilowatt Hour for PV and 5 ¢ per Killowatt Hour for Dispatchable CSP," pp. 2–6, 2017.

[3] P. Sochor and H. Akagi, "Theoretical comparison in energy-balancing capability between star- and delta-configured modular multilevel cascade inverters for utility-scale photovoltaic systems," *IEEE Trans. Power Electron.*, vol. 31, no. 3, pp. 1980–1992, 2016.

[4] NREL/Sandia/Sunspec Alliance SuNLaMP PV O&M Working Group, "Best Practices in Photovoltaic System Operations and Maintenance 2 nd Edition," no. December, 2016.

[5] A. Mohammadpour, L. Parsa, M. H. Todorovic, R. Lai, R. Datta, and L. Garces, "Series-input parallel-output modular-phase DC-DC converter with soft-switching and high-frequency isolation," IEEE Trans. Power Electron., vol. 31, no. 1, pp. 111–119, Jan. 2016.

[6] X. Hu and C. Gong, "A high gain input-parallel output-series DC/DC converter with dual coupled inductors," IEEE Trans. Power Electron., vol. 30, no. 3, pp. 1306–1317, Mar. 2015.

[7] R. Suryadevara and L. Parsa, "Full-Bridge ZCS-Converter-Based High-Gain Modular DC-DC Converter for PV Integration with Medium-Voltage DC Grids," *IEEE Trans. Energy Convers.*, vol. 34, no. 1, pp. 302–312, 2019.

[8] Y. Yu, G. Konstantinou, B. Hredzak, and V. G. Agelidis, "Power Balance of Cascaded H-Bridge Multilevel Converters for Large-Scale Photovoltaic Integration," *IEEE Trans. Power Electron.*, vol. 31, no. 1, pp. 292–303, 2016.

[9] M. Rabiul Islam, A. M. Mahfuz-Ur-Rahman, K. M. Muttaqi, and D. Sutanto, "State-of-The-Art of the Medium-Voltage Power Converter Technologies for Grid Integration of Solar Photovoltaic Power Plants," *IEEE Trans. Energy Convers.*, vol. 34, no. 1, pp. 372–384, 2019.

[10] S.B. Kjaer ; J.K. Pedersen ; F. Blaabjerg, "A review of single-phase grid-connected inverters for photovoltaic modules," *IEEE Trans. Ind. Appl.*, vol. 1, no. 9, pp. 521–525, 2014.

[11] H. Keyhani and H. A. Toliyat, "Single-stage multistring PV inverter with an isolated high-frequency link and soft-switching operation," *IEEE Trans. Power Electron.*, vol. 29, no. 8, pp. 3919–3929, 2014.

[12] H. Hu *et al.*, "A three-port flyback for PV microinverter applications with power pulsation decoupling capability," *IEEE Trans. Power Electron.*, vol. 27, no. 9, pp. 3953–3964, 2012.

[13] H. Athab, H. Zhu, B. Wu, D. Zhang, and Y. Gu, "PV Isolated Three-Port Converter and Energy Balancing Control Method for PV-Battery Power Supply Applications," *IEEE Trans. Ind. Electron.*, vol. 62, no. 6, pp. 1–1, 2014.

[14] M. Khodabandeh, E. Afshari, and M. Amirabadi, "A Single-Stage Soft-Switching High-Frequency AC-Link PV Inverter: Design, Analysis, and Evaluation of Si-Based and SiC-Based Prototypes," *IEEE Trans. Power Electron.*, vol. 34, no. 3, pp. 2312–2326, 2019.

[15] D. Divan, Z. An, and P. Kandula, "Soft-switching - The Key to High Power WBG Converters," 2018 Int. Power Electron. Conf. IPEC-Niigata - ECCE Asia 2018, no. Figure 1, pp. 4001–4008, 2018.

[16] R. Fu, T. Remo, R. Margolis, R. Fu, T. Remo, and R. Margolis, "2018 U . S . Utility-Scale Photovoltaics- Plus-Energy Storage System Costs Benchmark," *Natl. Renew. Energy Lab.*, no. November, p. 32, 2018.

[17] P. L. Denholm, R. M. Margolis, and J. D. Eichman, "Evaluating the Technical and Economic Performance of PV Plus Storage Power Plants," no. August, 2017.

[18] H. Chen and D. Divan, "Soft-Switching Solid-State Transformer (S4T)," IEEE Trans. Power Electron., vol. 33, no. 4, pp. 2933–2947, 2018.

[19] H. Hu, S. Harb, N. Kutkut, I. Batarseh, and Z. J. Shen, "A review of power decoupling techniques for microinverters with three different decoupling capacitor locations in PV systems," IEEE Trans. Power Electron., vol. 28, no. 6, pp. 2711–2726, 2013.

[20] N. Bilakanti, L. Zheng, R. P. Kandula, K. Kandasamy, and D. Divan, "Soft-Switching Isolated Tri-port Converter for Integration of PV, Storage and Single-Phase AC Grid," 2017 IEEE Energy Convers. Congr. Expo., pp. 482–489, 2017.

[21] L. Zheng, R. P. Kandula, K. Kandasamy, and D. Divan, "Fast Dynamic Control of Stacked Low Inertia Converters," 2018 IEEE Energy Convers. Congr. Expo. ECCE 2018, pp. 3126–3133, 2018.

[22] M. J. Mauger, R. P. Kandula, D. Divan, "Optimal Design of the Resonant Tank of the Soft-Switching Solid-State Transformer," 2019 IEEE Energy Convers. Congr. Expo. ECCE 2019.

[23] L. Zheng et al., "Modular Universal Converter for MVDC Applications," 2018 IEEE Energy Convers. Congr. Expo. ECCE 2018, pp. 5544–5551, 2018.

[24] X. Han, L. Zheng, R. P. Kandula, K. Kandasamy, M. Saeedifard, and D. Divan, "Real-Time Modeling and HIL Simulation of Stacked Low-Inertia Converters with Soft-Switching and Fast Dynamic Control," 2019 IEEE Energy Convers. Congr. Expo. ECCE 2019.